Supplementary material

Structural impact of GTP binding on downstream KRAS signaling

Dóra K. Menyhárd,[1] Gyula Pálfy,[1] Zoltán Orgován,[2] István Vida,[1] György M. Keserű,[2]* András Perczel[1]*

[1]Laboratory of Structural Chemistry and Biology & MTA-ELTE Protein Modelling Research Group, Institute of Chemistry, Eötvös Loránd University, Pázmány Péter sétány 1/A, 1117 Budapest, Hungary

[2]Medicinal Chemistry Research Group, Research Centre for Natural Sciences, Magyar tudósok körútja 2, Budapest 1117, Hungary

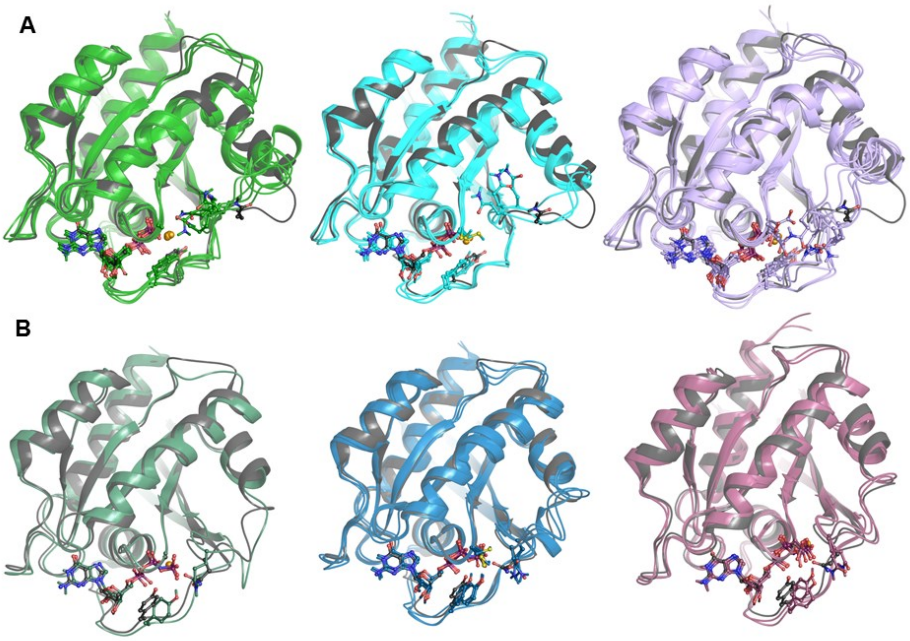

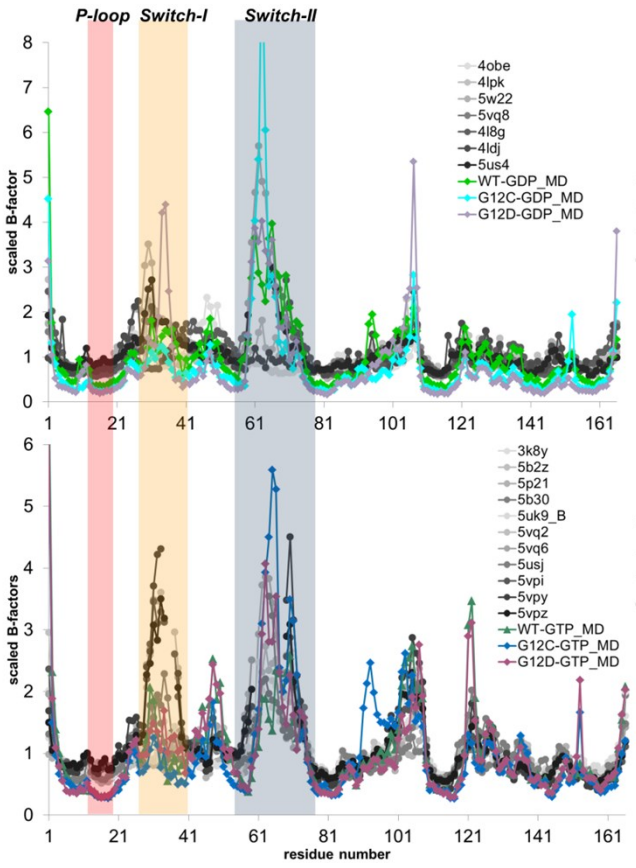

C

	core RMSD / Å	full RMSD / Å
WT-GDP	0.88	1.61
G12C-GDP	0.79	1.43
G12D-GDP	1.06	1.58

D

	core RMSD / Å	full RMSD / Å
WT-GTP	0.81	1.13
G12C-GTP	0.76	0.92
G12D-GTP	0.83	0.92

Suppl. Figure 1. Comparing the MD-derived and crystal structures of the RAS-GDP and -GTP complexes. (**A**) Mid-structures of the most populated clusters (clustered based on the conformation of the main-chain, accounting for at least 90% of the snapshots of the last 300ns of the simulations) of (**A**) KRAS-GDP and (**B**) KRAS-GTP (left: WT, middle: G12C, right: G12D) overlaid on the crystal structures used for building the starting models (4obe and 3k8y). Comparison of calculated and experimental B-factors of the (WT and mutant) (**C**) KRAS-GDP and (**D**) KRAS/HRAS-GTP/GTP-analogue complexes, and the RMSD (MD vs. the crystal structures: **4obe** and **3k8y**) of the main-chain atoms calculated for the core segments of the protein(helices and strands: residues 3-10, 16-26, 41-46, 48-57, 77-83, 86-104, 111-117, 126-137, 141-144, 152-166) and along the full sequence (except for 2 penultimate residues of the N- and C-terminal).

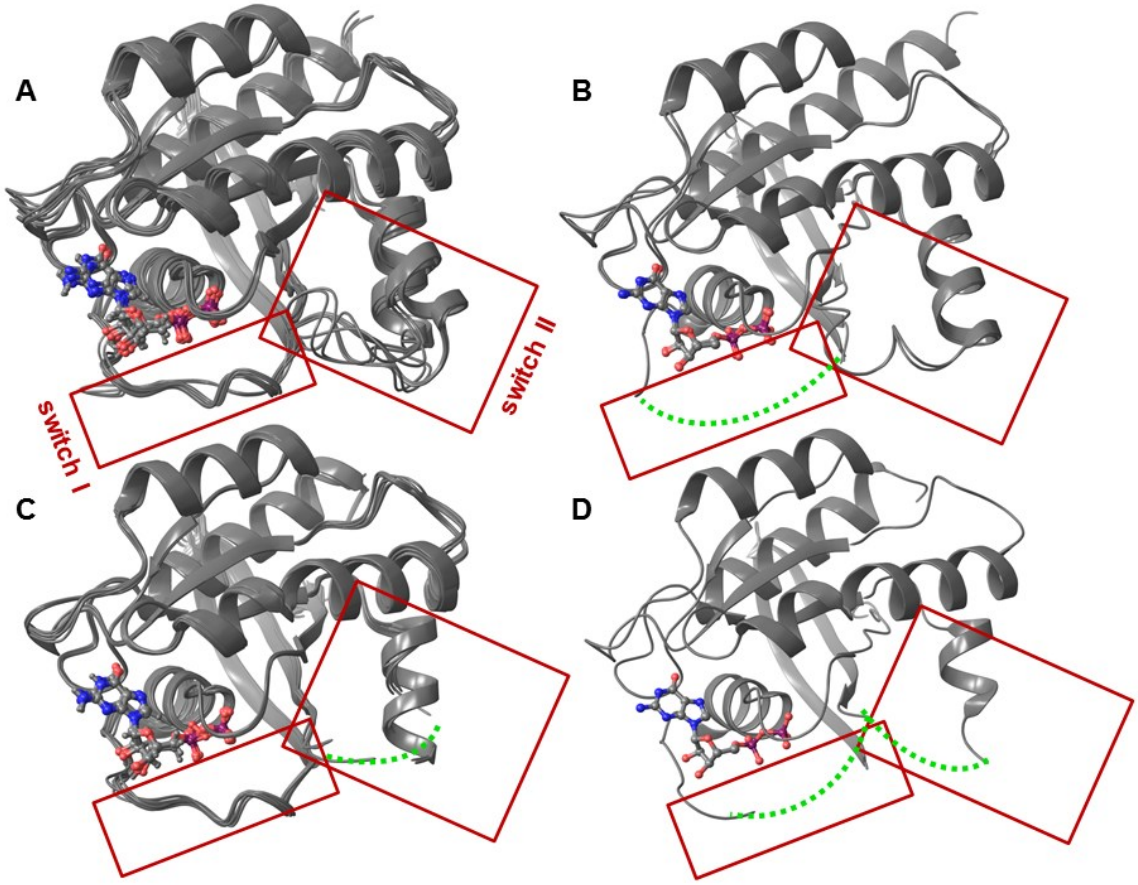

Suppl. Figure 2. KRAS-GDP complex crystal structures (showing the nucleotide explicitly). (**A**) Complexes where the entire sequence was well resolved: WT KRAS-GDP (structures with PDB codes: **4lpk**_chainB, **4obe**, **5w22**), G12A KRAS-GDP (**5vp7**), G12C KRAS-GDP (**4ldj**), G12R KRAS-GDP (**4ql3**), G12V KRAS-GDP (**4tq9**, **5uqw**_chainA), G13D KRAS-GDP (**4tq9**), D33E KRAS-GDP (**6asa**), A59G KRAS-GDP (**6ase**). (**B**) Entries where switch I region was unresolved in the electron density: WT KRAS-GDP (**5tb5**). (**C**) Entries where switch II region was unresolved in the electron density: WT KRAS-GDP (**4lpk**_chainA), G12A KRAS-GDP (**5vq0**), G12C KRAS-GDP (**4l8g, 4lwr**), G12D KRAS-GDP (**5us4**), G12V KRAS-GDP (**5uqw**), Q61A G12R KRAS-GDP (**5vq1**), Q61L G12R KRAS-GDP (**4wa7**). (**D**) Entry **5vq8** (WT KRAS-GDP) where both switch regions remained unresolved. (References of the crystal structures are listed at the end of the Supporting Information file.)

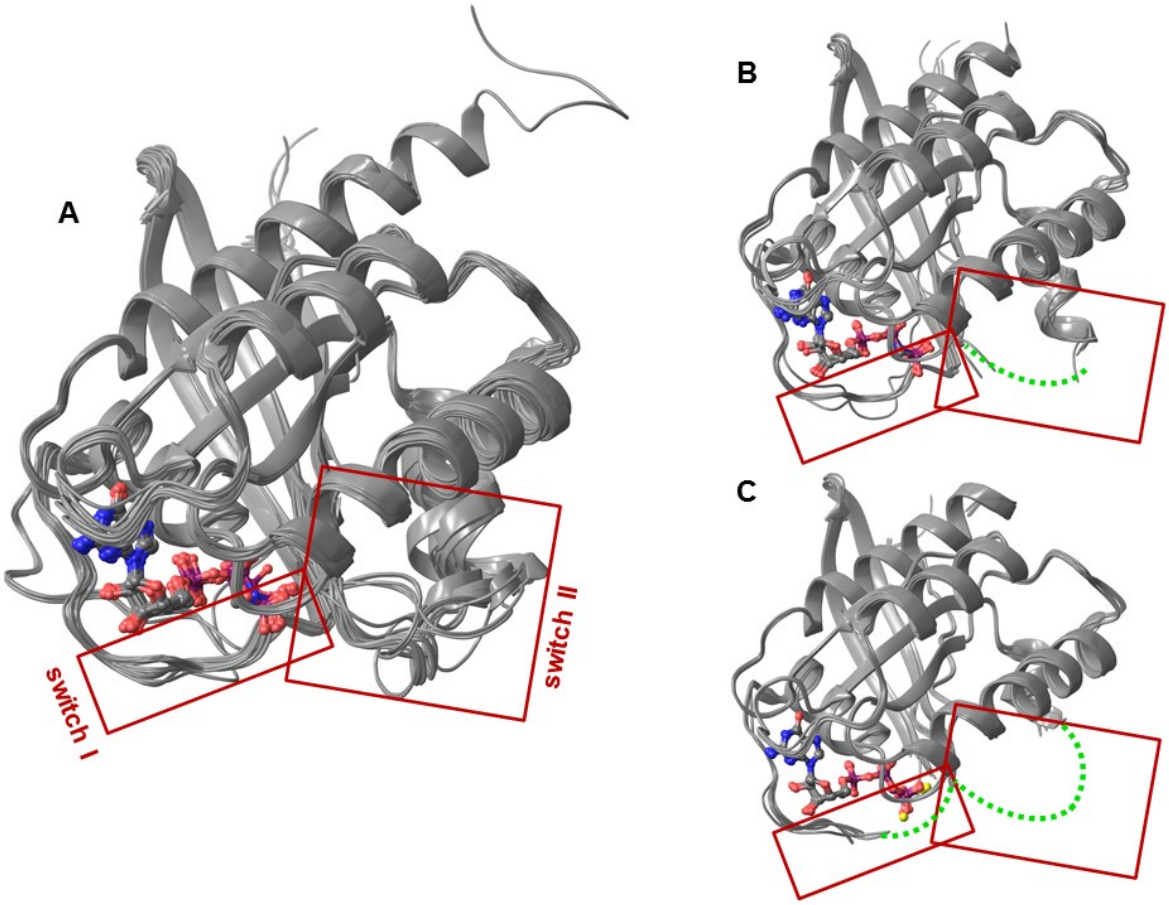

Suppl. Figure 3. KRAS/HRAS-GTP/GTP-analogue (GTPan) complex crystal structures (showing the nucleotide explicitly). (**A**) Complexes where the entire sequence was well resolved: WT HRAS-GTP (structure with PDB code: **1qra**), WT HRAS-GTPan (**1ctq, 2rge, 3k8y, 3l8z, 3lbh, 3tgp, 4efl, 5b2z, 5b30, 5p21**), G12D KRAS-GTPan (**4dsn**, **5usj_chainsB,C,E,F**), G12D HRAS-GTPan (**4efm**), G12V HRAS-GTPan (**4efn**), A59G KRAS-GTPan (**6bp1**), Q61H KRAS-GTPan (**3gft_chainA**), Q61L HRAS-GTPan (**2rgd**). (**B**) Entries where switch II region was unresolved in the electron density: WT KRAS-GTPan (**5uk9_chainB**), WT HRAS-GTPan (**4rsg**), G12D KRAS-GTPan (**5usj_chains A, D**), Q61H KRAS-GTPan (**3gft_chains B, C, E**). (**C**) Entries where both switch regions remained unresolved: KRAS WT-GTP (**5vq2**), KRAS WT-GTPan (**5vq6**), KRAS G12A-GTP (**5vpi, 5vpz**), KRAS G12A-GTPan (**5vpy**), KRAS Q61H-GTPan (**3gft_chains D, F**). (References of the crystal structures are listed at the end of the Supporting Information file.)

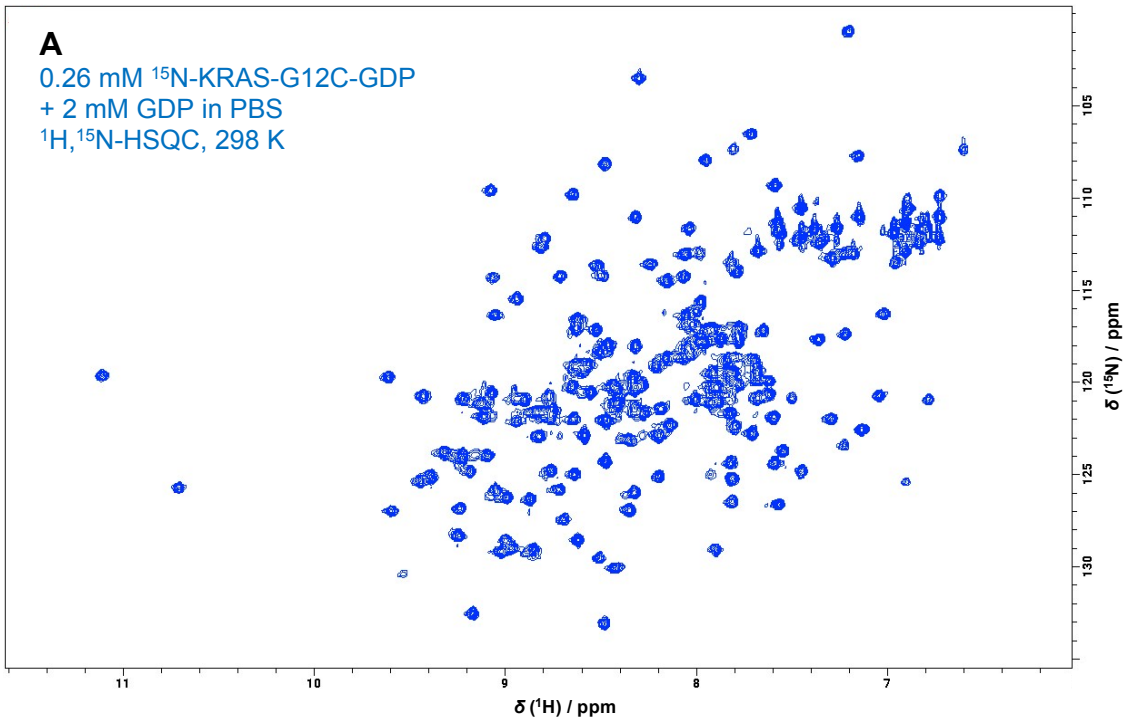
A
0.26 mM 15N-KRAS-G12C-GDP
+ 2 mM GDP in PBS
1H,15N-HSQC, 298 K
δ (1H) / ppm
δ (15N) / ppm

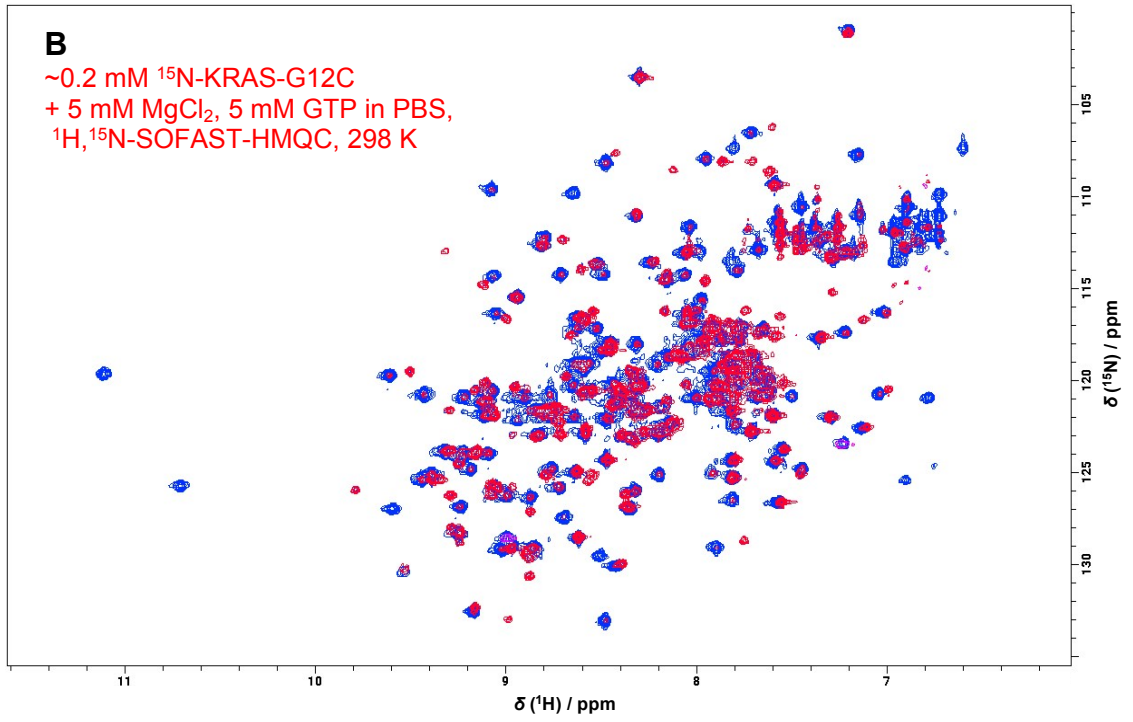
B
~0.2 mM 15N-KRAS-G12C
+ 5 mM MgCl2, 5 mM GTP in PBS,
1H,15N-SOFAST-HMQC, 298 K
δ (1H) / ppm
δ (15N) / ppm

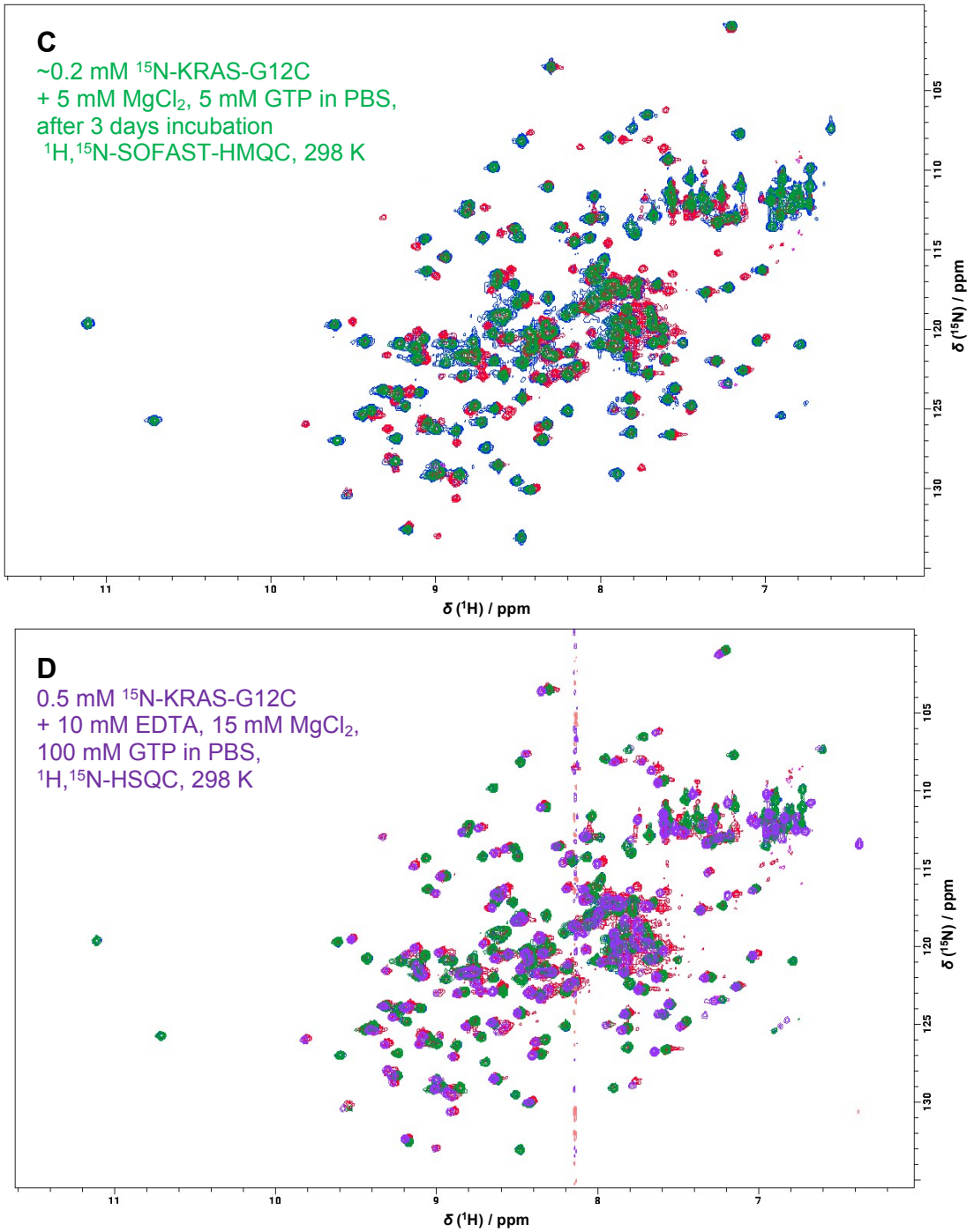

Suppl. Figure 4. (**A**) $^{1}H,^{15}N$-HSQC spectrum (colored blue) of 0.26 mM ^{15}N-KRAS-G12C-GDP with 2 mM GDP in buffer, PBS, pH = 7.4. (**B**) $^{1}H,^{15}N$-SOFAST-HMQC spectrum (colored red) of the same sample after adding 10 mM EDTA, then 5 times 3-fold dilution in PBS and subsequent concentration (in entirety a 243-fold dilution of the buffer) removing the most of GDP from the solution, then adding 5 mM GTP and 5 mM $MgCl_2$ at pH = 7.4, recorded after a while. The spectrum is overlaid onto the spectrum (A). There are new peaks in the spectrum, but the same peaks can be detected as well, which are found in spectrum (A) indicating that a mixture of KRAS-G12C-GTP and KRAS-G12C-GDP are present in the sample. (**C**) $^{1}H,^{15}N$-SOFAST-HMQC spectrum (colored green) of the sample (B) after 3 days incubation at 298 K, overlaid onto spectrum (A) and (B). The green signals are completely overlapped with blue signals indicating that after 3 days incubation, only KRAS-G12C-GDP form is present in the NMR sample due to the GTP-hydrolysis of GTPase KRAS protein. (**D**) $^{1}H,^{15}N$-HSQC spectrum (colored purple) of a new sample containing 0.5 mM ^{15}N-KRAS-G12C protein, 10 mM EDTA in PBS, and consequently added 15 mM MgCl2, ~100 mM GTP, pH = 7.4 overlaid on spectrum (A), (B) and (C). The purple peaks are completely overlapped with those red peaks which are not found in spectra (A) and (C), these peaks disappeared from spectrum (B) after 3 days incubation indicating that this spectrum only contains signals of KRAS-G12C-GTP. All spectra were recorded at 298 K on a Bruker Avance III 700 MHz spectrometer.

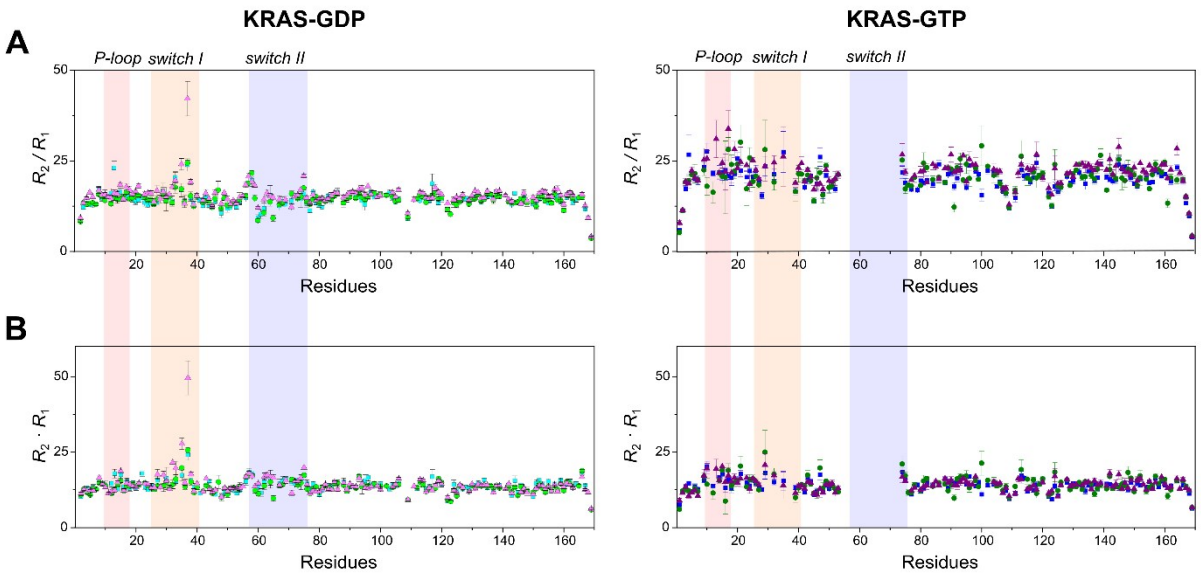

Suppl. Figure 5. (**A**) R_2/R_1 and (**B**) $R_2 \cdot R_1$ values of KRAS WT (light green/green), G12C mutant (cyan/blue), G12D mutant (lilac/purple) in GDP-bound (left) and GTP-bound forms (right). P-loop (light red, residues 10-17), switch I (yellow, residues 25-40) and switch II (light blue, residues 57-76) are shown in colored rectangles.

KRAS-WT-GDP	R_1 (s^{-1})	R_2 (s^{-1})	HetNOE	S^2	τ_e (ps)	R_{ex} (s^{-1})	Model	$J(\omega_h)$ / ps rad^{-1}
His27	0.98 ± 0.02	14.07 ± 0.18	0.88	0.87 ± 0.01	-	-	1	1.84
Phe28	N.D.	N.D.	N.D.	N.D.	N.D.	N.D.	N.D.	N.D.
Val29	0.94 ± 0.01	14.74 ± 0.71	0.77	0.82 ± 0.01	-	-	1	3.41
Asp30	1.04 ± 0.01	14.45 ± 0.50	0.72	0.88 ± 0.01	42 ± 16	-	2	4.5
Glu31	0.94 ± 0.05	14.15 ± 0.42	0.91	0.86 ± 0.02	-	-	1	1.39
Tyr32	1.03 ± 0.01	13.83 ± 0.52	0.39	0.80 ± 0.01	107 ± 12	-	2	9.77
Asp33	0.95 ± 0.04	16.85 ± 1.35	0.79	0.83 ± 0.03	-	3.49 ± 1.45	3	3.1
Pro34	N.D.	N.D.	N.D.	N.D.	N.D.	N.D.	N.D.	N.D:
Thr35	1.07 ± 0.01	18.44 ± 0.71	0.81	0.93 ± 0.01	-	3.42 ± 0.71	3	3.22
Ile36	0.99 ± 0.02	13.61 ± 0.40	0.78	0.86 ± 0.02	-	-	1	3.35
Glu37	1.03 ± 0.01	25.04 ± 0.76	0.79	0.89 ± 0.01	-	10.68 ± 0.79	3	3.38

KRAS-G12C-GDP	R_1 (s^{-1})	R_2 (s^{-1})	HetNOE	S^2	τ_e (ps)	R_{ex} (s^{-1})	Model	$J(\omega_h)$ / ps rad^{-1}
His27	1.07 ± 0.04	14.61 ± 0.26	0.80	0.91 ± 0.02	-	-	1	3.39
Phe28	N.D.	N.D.	N.D.	N.D.	N.D.	N.D.	N.D.	N.D.
Val29	0.91 ± 0.06	15.15 ± 1.76	0.83	0.82 ± 0.05	-	-	1	2.37
Asp30	1.06 ± 0.15	15.34 ± 2.73	0.73	0.92 ± 0.10	64 ± 97	-	2	4.48
Glu31	N.D.	N.D.	N.D.	N.D.	N.D.	N.D.	N.D.	N.D.
Tyr32	1.02 ± 0.06	14.13 ± 1.17	0.42	0.81 ± 0.04	113 ± 43	-	2	9.17
Asp33	0.86 ± 0.04	17.53 ± 1.01	0.82	0.75 ± 0.04	-	5.47 ± 1.17	3	2.47
Pro34	N.D.	N.D.	N.D.	N.D.	N.D.	N.D.	N.D.	N.D.
Thr35	1.01 ± 0.08	17.13 ± 1.26	0.80	0.96 ± 0.05	-	-	1	3.24

Ile36	1.01 ± 0.09	14.08 ± 0.74	0.75	0.87 ± 0.04	-	-	1	3.96
Glu37	1.00 ± 0.05	23.97 ± 1.25	0.76	0.88 ± 0.05	-	9.83 ± 1.45	3	3.80

KRAS-G12D-GDP	R_1 (s^{-1})	R_2 (s^{-1})	HetNOE	S^2	τ_e (ps)	R_{ex} (s^{-1})	Model	$J(\omega_h)$ / ps rad^{-1}
His27	1.02 ± 0.03	17.18 ± 1.49	0.86	0.94 ± 0.02	-	-	1	2.22
Phe28	0.96 ± 0.04	13.95 ± 0.84	0.78	0.86 ± 0.03	-	-	1	3.25
Val29	1.03 ± 0.04	16.93 ± 1.06	0.86	0.95 ± 0.03	-	-	1	2.31
Asp30	1.01 ± 0.01	15.22 ± 0.48	0.74	0.92 ± 0.01	-	-	1	4.1
Glu31	0.90 ± 0.03	14.17 ± 0.24	0.81	0.84 ± 0.01	-	-	1	2.7
Tyr32	1.10 ± 0.02	19.58 ± 0.56	0.50	0.88 ± 0.02	303 ± 94	4.65 ± 0.63	4	8.68
Asp33	1.00 ± 0.09	19.67 ± 1.37	0.80	1.00 ± 0.06	-	-	1	3.18
Pro34	N.D.	N.D.	N.D.	N.D.	N.D.	N.D.	N.D.	N.D.
Thr35	1.07 ± 0.04	25.86 ± 1.46	0.72	0.94 ± 0.03	125 ± 116	9.9 ± 1.6	4	4.75
Ile36	1.06 ± 0.07	14.02 ± 0.59	0.82	0.86 ± 0.03	-	-	1	2.94
Glu37	1.08 ± 0.08	45.70 ± 3.86	0.80	0.99 ± 0.07	-	29.1 ± 4.1	3	3.33

KRAS-WT-GTP	R_1 (s^{-1})	R_2 (s^{-1})	HetNOE	S^2	τ_e (ps)	R_{ex} (s^{-1})	Model	$J(\omega_h)$ / ps rad^{-1}
His27	0.83 ± 0.02	15.15 ± 0.59	0.64	0.81 ± 0.02	40.9 ± 8.5	-	2	4.58
Phe28	N.D.	N.D.	N.D.	N.D.	N.D.	N.D.	N.D.	N.D.
Val29	0.94 ± 0.13	26.51 ± 6.72	0.91	1.00 ± 0.13	-	-	1	1.37
Asp30	N.D.	N.D.	N.D.	N.D.	N.D.	N.D.	N.D.	N.D.
Glu31	N.D.	N.D.	N.D.	N.D.	N.D.	N.D.	N.D.	N.D.
Tyr32	0.96 ± 0.09	18.39 ± 1.21	0.93	0.96 ± 0.05	-	-	1	1.10
Asp33	N.D.	N.D.	N.D.	N.D.	N.D.	N.D.	N.D.	N.D.

Pro34	N.D.	N.D.	N.D.	N.D.	N.D.	N.D.	N.D.	N.D.
Thr35	N.D.	N.D.	N.D.	N.D.	N.D.	N.D.	N.D.	N.D.
Ile36	N.D.	N.D.	N.D.	N.D.	N.D.	N.D.	N.D.	N.D.
Glu37	N.D.	N.D.	N.D.	N.D.	N.D.	N.D.	N.D.	N.D.

KRAS-G12C-GTP	R_1 (s^{-1})	R_2 (s^{-1})	HetNOE	S^2	τ_e (ps)	R_{ex} (s^{-1})	Model	$J(\omega_h)$ / ps rad^{-1}
His27	0.85 ± 0.03	16.04 ± 1.01	0.72	0.84 ± 0.03	29 ± 11	-	2	3.7
Phe28	0.90 ± 0.04	13.92 ± 0.49	0.84	0.78 ± 0.02	-	-	1	2.25
Val29	0.88 ± 0.04	20.67 ± 2.11	0.69	0.93 ± 0.04	-	-	1	4.25
Asp30	N.D.	N.D.	N.D.	N.D.	N.D.	N.D.	N.D.	N.D.
Glu31	N.D.	N.D.	N.D.	N.D.	N.D.	N.D.	N.D.	N.D.
Tyr32	0.84 ± 0.02	17.94 ± 1.15	0.75	0.87 ± 0.02	-	-	1	3.33
Asp33	N.D.	N.D.	N.D.	N.D.	N.D.	N.D.	N.D.	N.D.
Pro34	N.D.	N.D.	N.D.	N.D.	N.D.	N.D.	N.D.	N.D.
Thr35	0.75 ± 0.04	20.60 ± 4.12	0.81	0.78 ± 0.04	-	-	1	2.21
Ile36	N.D.	N.D.	N.D.	N.D.	N.D.	N.D.	N.D.	3.7
Glu37	N.D.	N.D.	N.D.	N.D.	N.D.	N.D.	N.D.	2.25

KRAS-G12D-GTP	R_1 (s^{-1})	R_2 (s^{-1})	HetNOE	S^2	τ_e (ps)	R_{ex} (s^{-1})	Model	$J(\omega_h)$ / ps rad^{-1}
His27	0.84 ± 0.03	16.82 ± 0.77	0.76	0.87 ± 0.03	26 ± 13	-	2	3.19
Phe28	N.D.	N.D.	N.D.	N.D.	N.D.	N.D.	N.D.	N.D.
Val29	0.94 ± 0.07	22.09 ± 3.54	0.60	0.93 ± 0.02	273 ± 480	-	2	5.84
Asp30	N.D.	N.D.	N.D.	N.D.	N.D.	N.D.	N.D.	N.D.
Glu31	N.D.	N.D.	N.D.	N.D.	N.D.	N.D.	N.D.	N.D.
Tyr32	0.84 ± 0.05	20.58 ± 1.03	0.91	0.96 ± 0.04	-	-	1	1.12

Asp33	N.D.	N.D.	N.D.	N.D.	N.D.	N.D.	N.D.	N.D.
Pro34	N.D.	N.D.	N.D.	N.D.	N.D.	N.D.	N.D.	N.D.
Thr35	0.73 ± 0.12	19.13 ± 5.16	0.46	0.76 ± 0.11	52 ± 33	-	2	2.94
Ile36	N.D.	N.D.	N.D.	N.D.	N.D.	N.D.	N.D.	N.D.
Glu37	N.D.	N.D.	N.D.	N.D.	N.D.	N.D.	N.D.	N.D.

Suppl. Table 1. Per residue values of the measured relaxation parameters, and the derived Modelfree parameters for the most interesting switch I region. (N.D.stands for: no data)

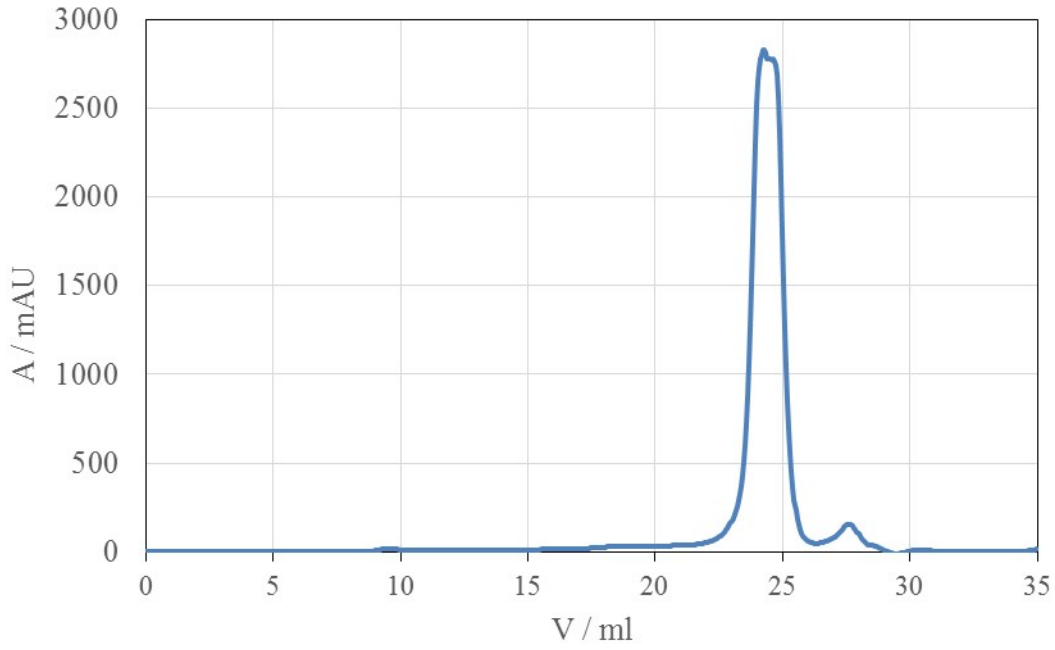

Suppl. Figure 6. Size-exclusion chromatogram of KRAS G12C nucleotide-free form. No significant peaks appear in the high molecular weight range, which suggests that during the purification process aggregation of the samples does not take place.

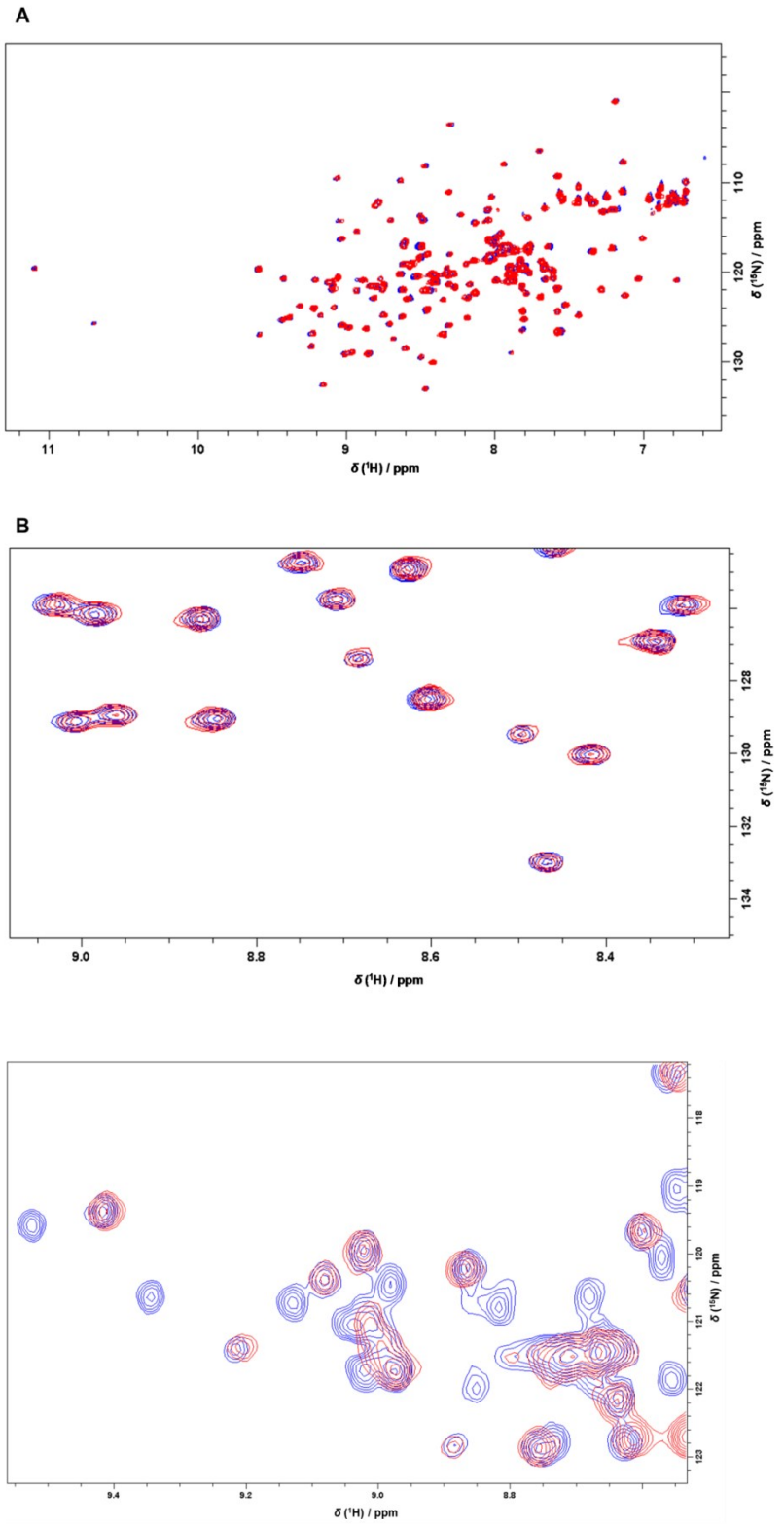

Suppl. Figure 7. (**A**) Overlaid $^{1}H,^{15}N$-HSQC spectra of ^{15}N-KRas-G12C-GDP in buffer that contains 2 mM (blue) and. 100 mM GDP, measured at 298 K on a Bruker Avance III 700 MHz spectrometer. (**B**) A zoom of the overlaid spectra shows signals being practically unaffected by the change in the GDP concentration. (**C**) A zoom of overlaid $^{1}H,^{15}N$-HSQC spectra of ^{15}N-KRAS-G12C-GTP in buffer that contains 5 mM (blue) and cca. 100 mM (red). In the blue spectrum the extra peaks belong to the emerging GDP-bound form due to GTP-hydrolysis. There is no significant difference between the linewidth measured in presence of small and large concentration of GTP.

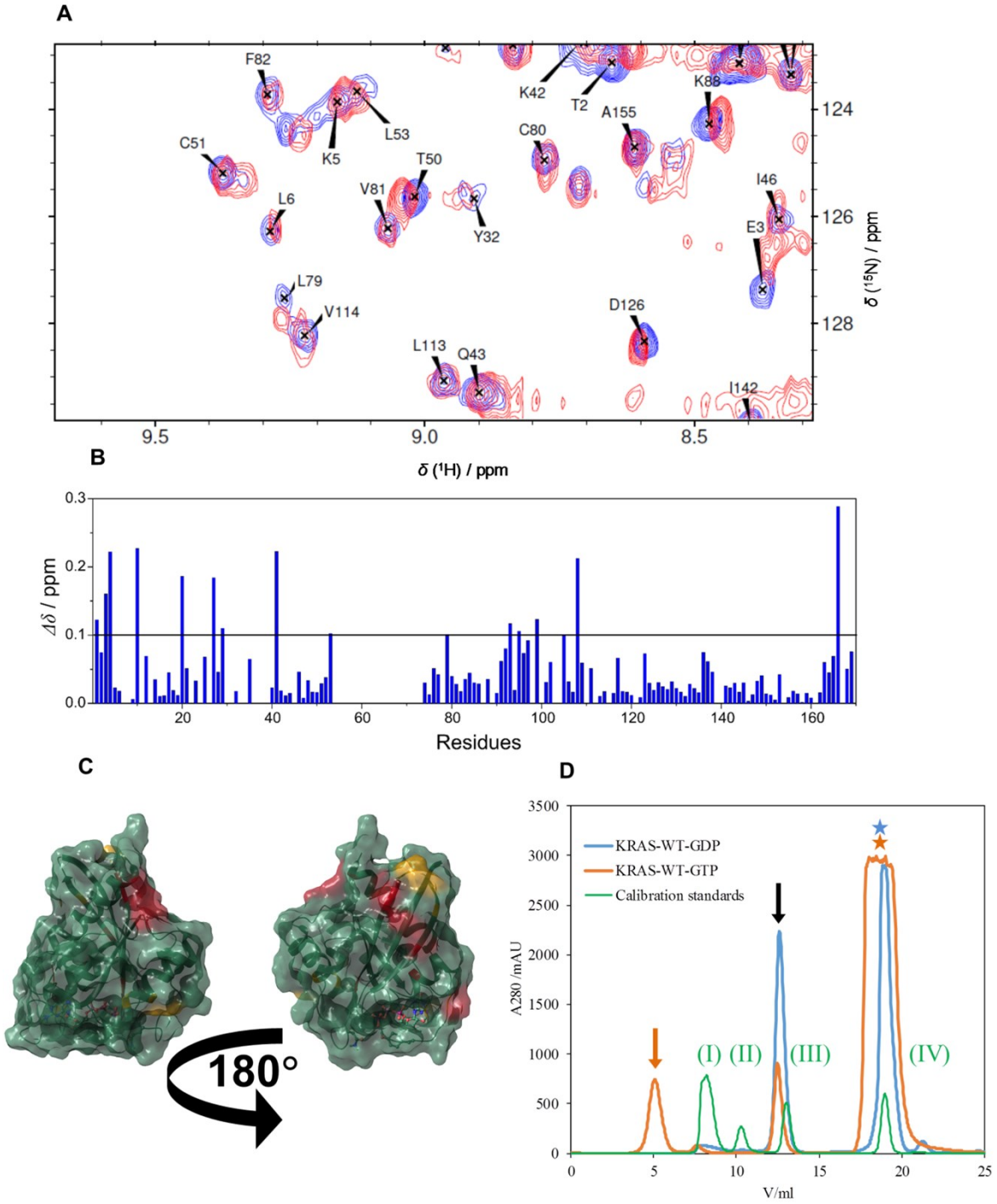

Suppl. Figure 8. (**A**) A section of the overlaid $^{1}H,^{15}N$-HSQC and $^{1}H,^{15}N$-SOFAST-HMQC spectra (neighbors of Tyr32) of ^{15}N-KRAS-G12C-GTP in samples containing 300 µM (blue) and 30 µM (red) protein, measured at 298 K on a Bruker Avance III 700 MHz spectrometer. (**B**) Combined chemical shift difference ($\Delta\delta$) values between $^{1}H,^{15}N$-HSQC resonances recorded at 30 and 300 µM ^{15}N-KRAS-G12C-GTP in function of the sequence. The black line at 0.1 ppm indicates the arbitrary limit used for selecting the residues that suffered the most significant changes.(**C**) Residue effected most significantly ($\Delta\delta$>0.15: red) and moderately (0.1<$\Delta\delta$<0.15: yellow) by the change in protein concentration, shown on the surface of KRAS. (**D**) Gel filtration chromatograms of GDP- (blue), GTP-bound (orange) KRAS-WT and calibration standard solution (green). Superdex 75 Increase 10/300 GL column was used with PBS buffer as eluent. Gel Filtration Standard (Bio-Rad) contained γ-globulin (I, 158 kDa), ovalbumin (II, 44 kDa), myoglobin (III, 17 kDa) and vitamin B12 (IV, 1.35 kDa). Chromatogram of KRAS-WT-GDP sample indicated presence of monomer KRAS-GDP (black arrow) and excess GDP (blue star). On the other hand, KRAS-WT-GTP samples contained –beside the monomeric form (black arrow) and excess GTP (orange star) - a third peak with molecular weight greater than 158 kDa (orange arrow), which likely belongs to an oligomer state.

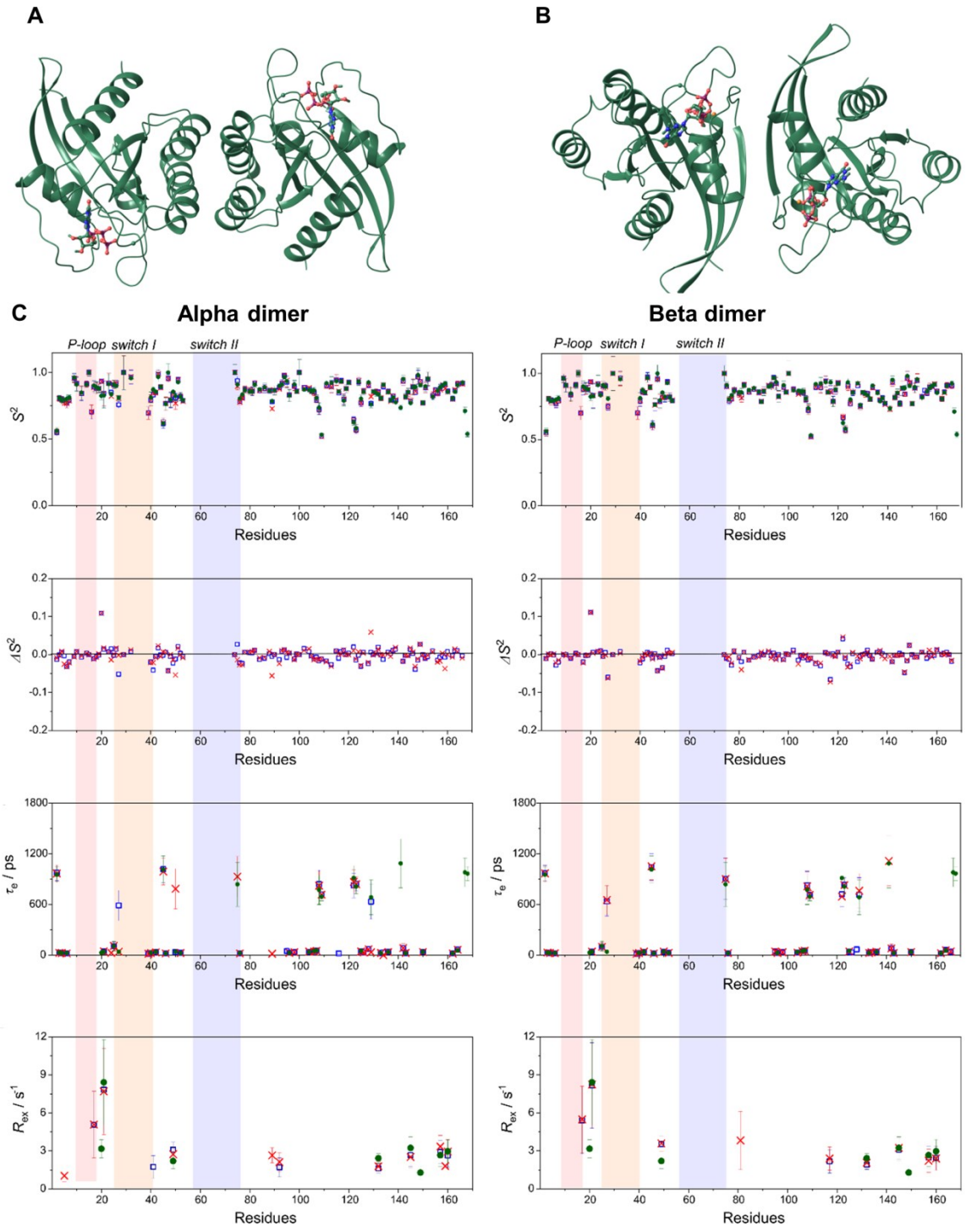

Suppl. Figure 9. Models of (**A**) α- and (**B**) β-homodimer of KRAS-WT-GTP using our MD derived structure (mid-structure of the most populated cluster), following the model building process presented in S. Muratcioglu et al,.Strucutre, 2015, 23(7): 1325–1335, relying of PDB structures: 4a9e (Chung, C.W., Dean, A.W., Woolven, J.M., Bamborough, P. (2012) J Med Chem 55: 576) and 2erx (Papagrigoriou, E., Yang, X., Elkins, J., Niesen, F.E., Burgess, N., Salah, E., Fedorov, O., Ball, L.J., von Delft, F., Sundstrom, M., Edwards, A., Arrowsmith, C., Weigelt, J., Doyle, D. *to be published*)). (**C**) Comparison of model free analysis of GTP-bound KRAS WT in monomer form (isotropic approach, indicated as green circles) α-dimer (using axially anisotropic approach: chain A in blue squares, chain B as red crosses) and β-dimer (using axially anisotropic approach : chain A in blue squares, chain B as red crosses) all of them derived from Lipari-Szabo Model-free formalism. P-loop (light red, residues 10-17), switch I (yellow, residues 25-40) and switch II (light blue, residues 57-76) are shown in colored rectangles. The obtained global correlation time (τ_c) was determined to be 12.3 ns for α-homodimer, 12.2 ns for β-homodimer, while 12.3 ns for monomer/isotropic approach, which is again not a significant change.

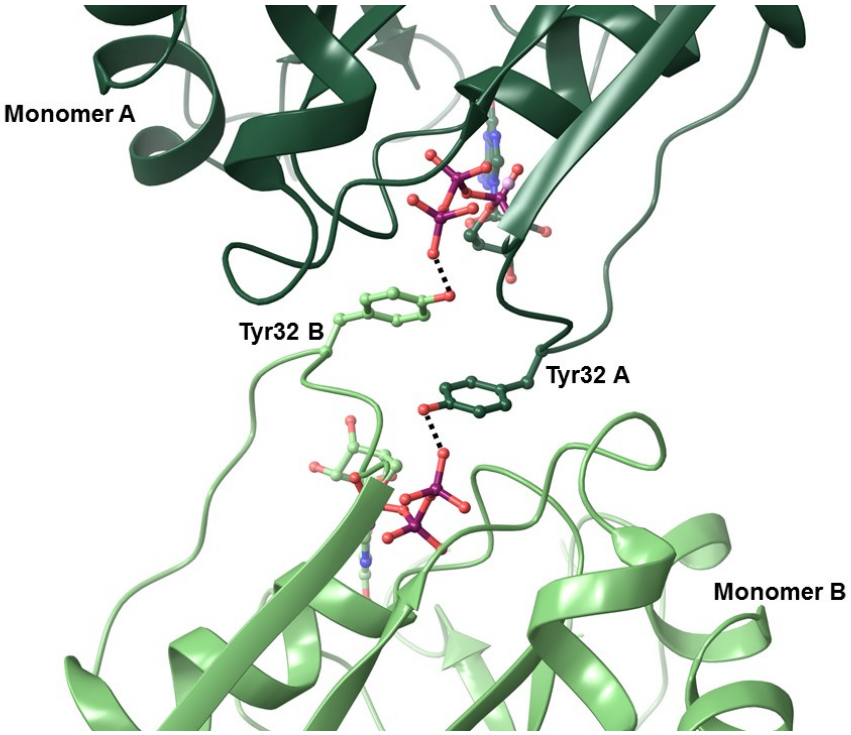

Suppl. Figure 10. Tyr32 interacting with the GTP (O1G atom of the γ-phosphate) of the neighboring monomer in the crystal structure of the HRAS-GTP complex (PDB code: **1qra** (see end of Suppl. Info file)).

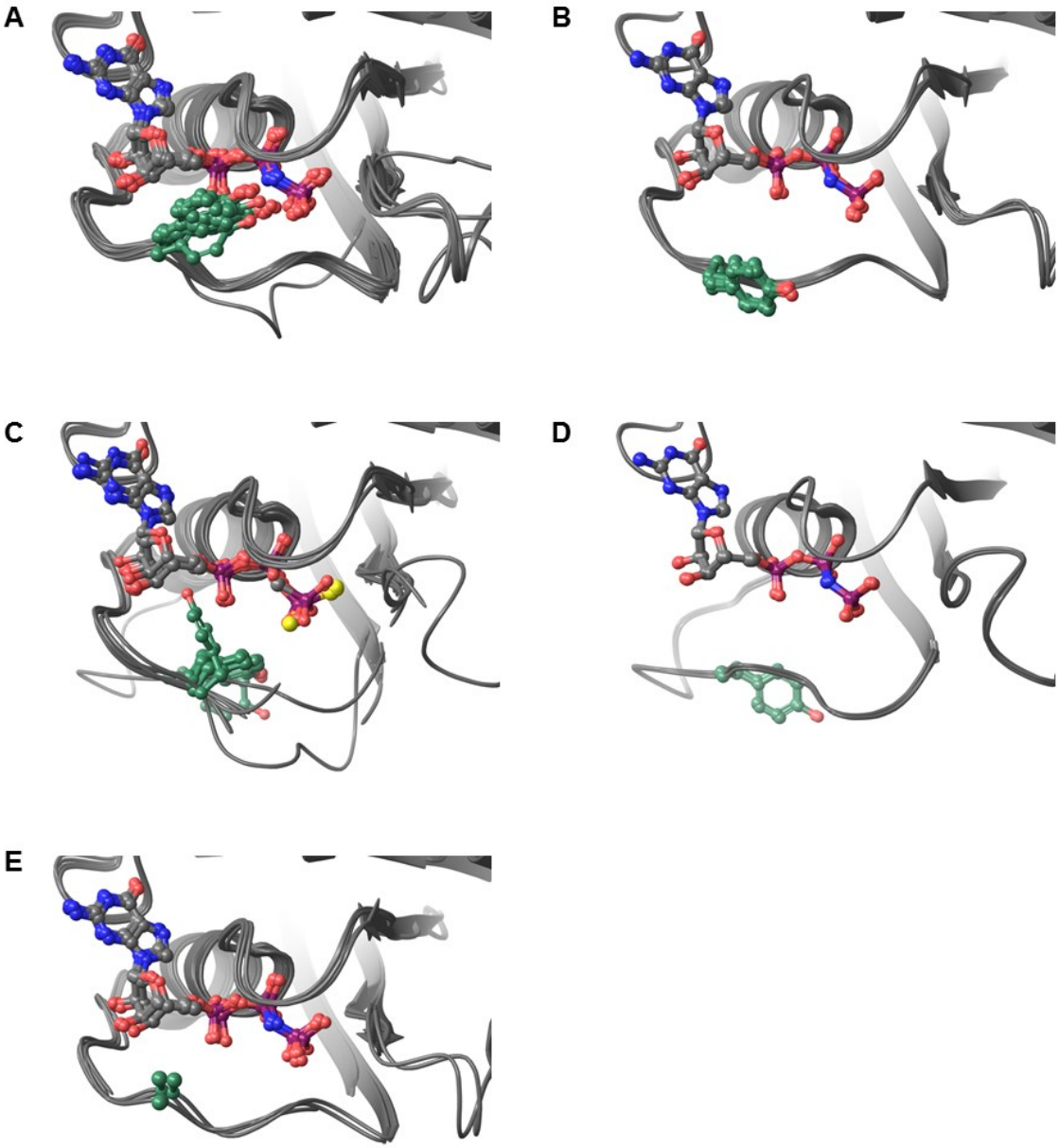

Suppl. Figure 11. The different orientation and position of Tyr32 in various RAS_GTP/GTP-analogue complexes. (**A**) Bound to, or located near the γ-phosphate of GTP (distance of Tyr32-OH.....O1G* of GTP: < 4Å): WT HRAS-GTPan (structures with PDB code: **2rge, 3k8y, 3l8z, 3lbh, 5b2z, 5b30**), G12A KRAS -GTP (**5vpi),** G12D KRAS-GTPan (**4dsn**, **5usj_chainsA,C,D**), Q61H KRAS-GTPan (**3gft_chainA,B,E**), Q61L HRAS-GTPan (**2rgd**). (**B**) Cross- bound to the γ-phosphate of the GTP of a neighboring monomer (distance of Tyr32-OH.....O1G of GTP: ~10-12Å) (see also Suppl. Fig. 4): WT HRAS-GTP (**1qra**), WT HRAS-GTPan (**1ctq, 3tgp, 4rsg, 5p21**). (**C**) Tyr32 within effector binding pocket, very much like in the GDP-bound states (distance of Tyr32-OH.....O1G of GTP: > 13Å): WT KRAS-GTP (**5vq2**), WT KRAS-GTPan (**5uk9_chainB, 5vq6, 5vpy, 5vpz**), A59G KRAS-GTPan (**6bp1**). (**D**) Tyr32 in the inactive conformation of RAS-GTP (distance of Tyr32-OH.....O1G of GTP: ~ 13.7 Å): WT HRAS-GTPan(4efl), G12D HRAS-GTPan (**4efn**), G12V HRAS-GTPan (**4efm**). (**E**) Partially and fully undetermined Tyr32: G12D KRAS-GTPan (**5usj_chainsB,F**), G61H KRAS-GTPan (**3gft_chainsC,D,F**). (*: O1G is the oxygen of the γ-phosphate that is not bound to either Mg^{2+} or Lys16.) (References of the crystal structures are listed at the end of the Supporting Information file.)

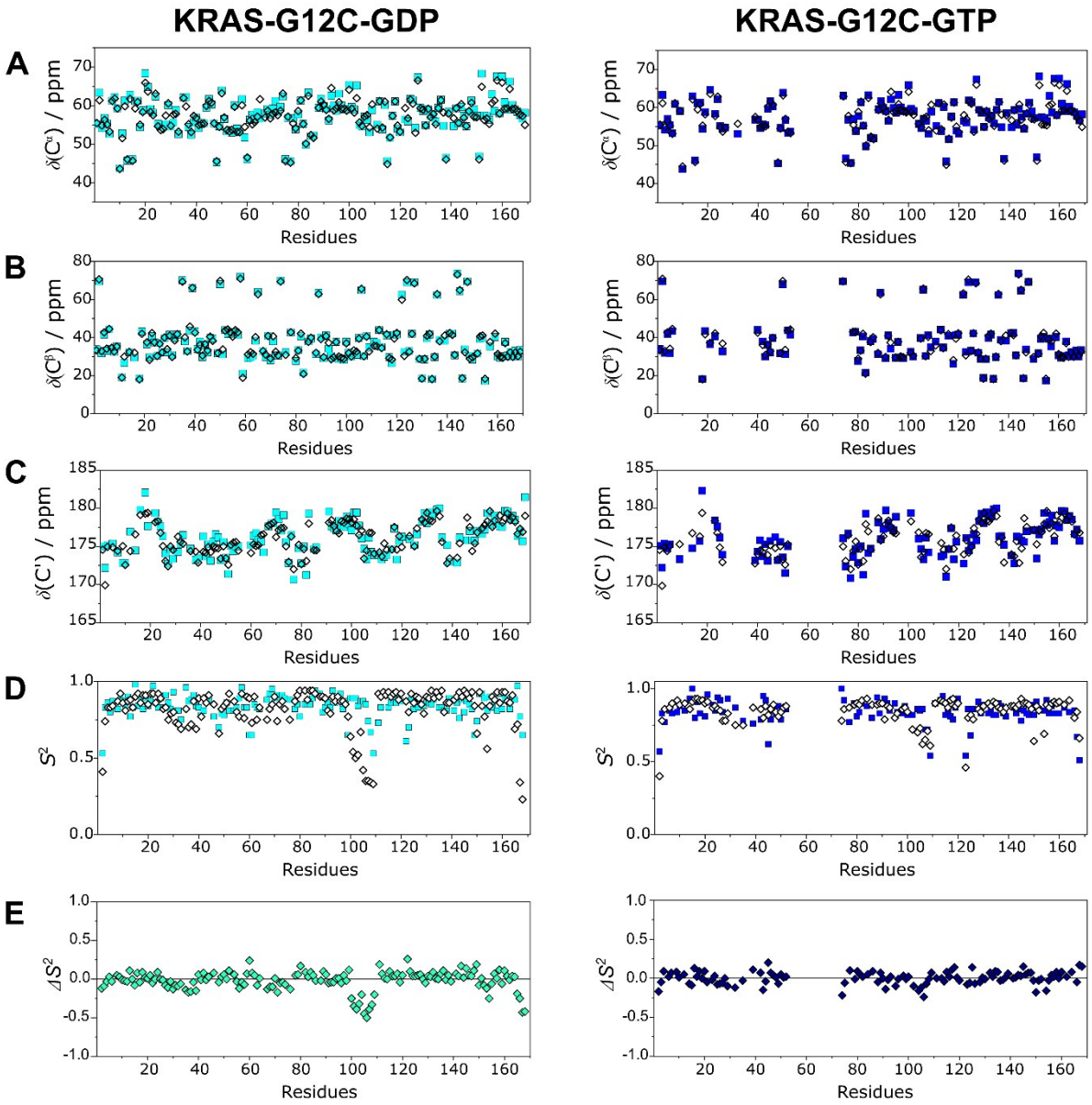

Suppl. Figure 12. Comparison of experimental and calculated (from MD ensemble using CoNSEnsX+ server) chemical shifts ((**A**) C^{α}, (**B**) C^{β} and (**C**) C') and (**D**) S^2 values as well as the difference between the calculated (MD derived) and experimental S^2 values (ΔS^2) for KRAS-G12C in GDP-bound (left) and GTP-bound (right) forms. Experimental values are depicted in cyan and blue (GDP- and GTP-bound forms, respectively), while the values belonging to the calculated forms are shown as empty diamonds in every graph.

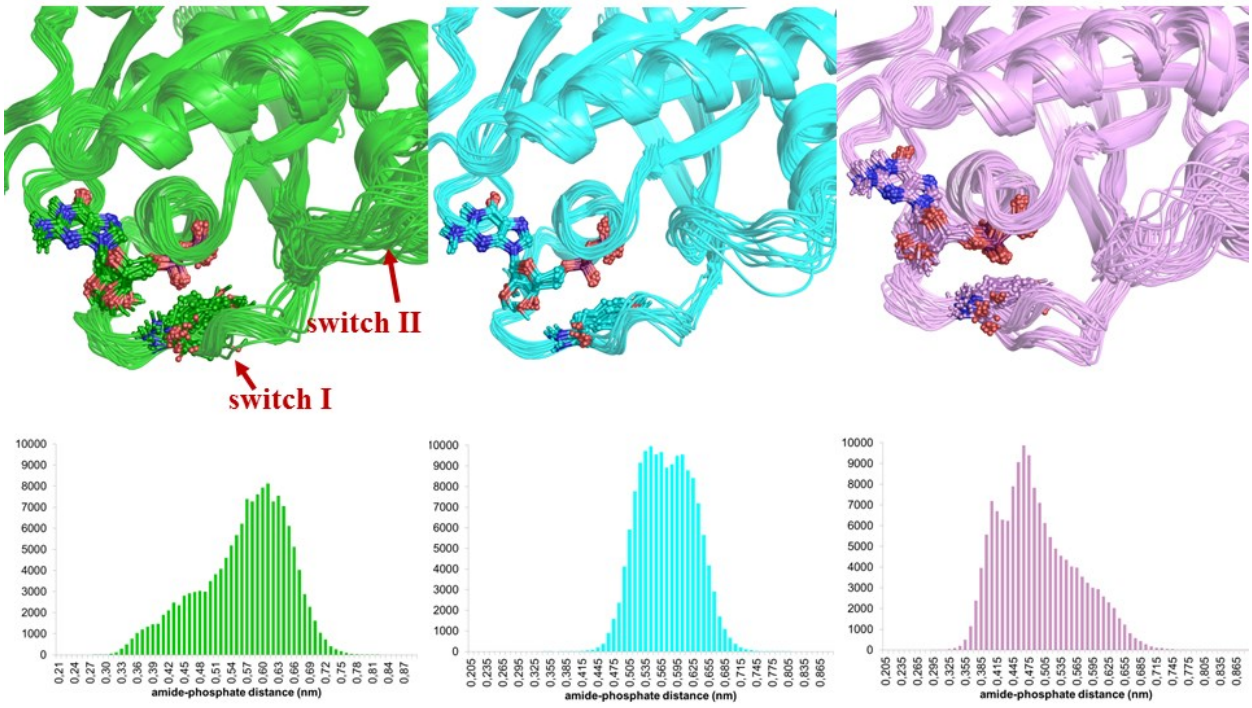

Suppl. Figure 13. The conformational and electrostatic heterogeneity of the backbone amide H of Tyr32 in the WT- (green), G12c (cyan) and G12D(lilac)-KRAS-GDP complexes. The ensembles are formed of the mid-structures of clusters based on the conformation of the main-chain in the residue 10-48 region, accounting for at least 90% of the snapshots of the last 300 ns of the simulations.

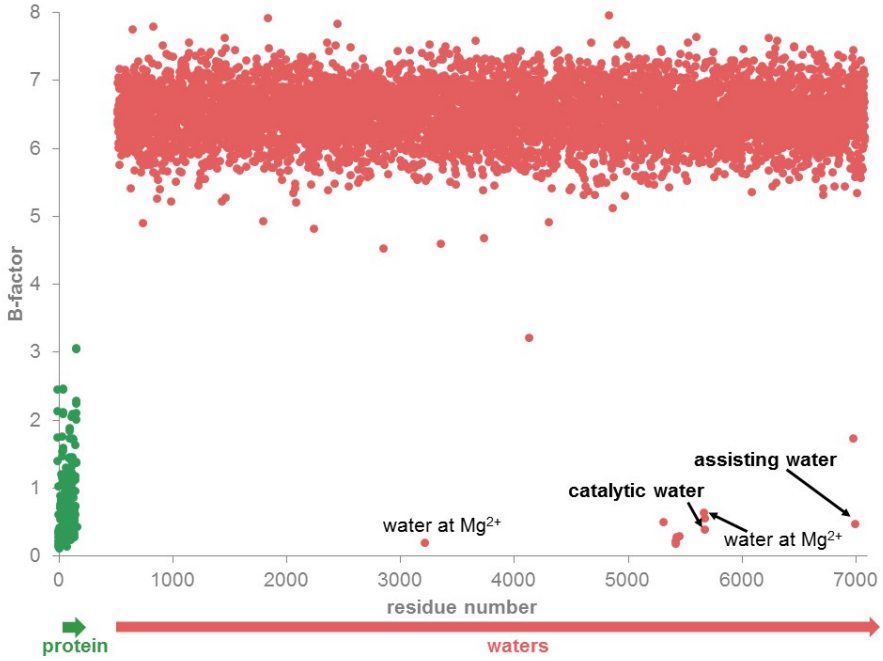

Suppl. Figure 14. MD-derived (normalized) B-factors of the WT-KRAS-GTP system (for all protein (green) and solvent (red) residues) demonstrating the capture of the catalytic and assisting waters. Waters with low (< 4, protein-like) B-factors are those that are securely bound within the protein matrix. Beside the catalytic (Wat5691) and assisting water (Wat7011) and the two waters completing the coordination sphere of the Mg^{2+}-ion (Wat3232, Wat5685), only six other structural water were found: Wat4142 coordinated by Glu76,His166; Wat5323 between Asp33 and O2A of GTP; Wat5434, Wat5435, Wat5463 trapped in the spacious pocket lined by Val8, Leu19, Leu23, Ile65, Leu79, Val152, Phe156; Wat5684 near Tyr64, Ser65; Wat5440 near Ala11, Val81, Ser89 and Wat6994 at Thr58 and O1G of GTP.

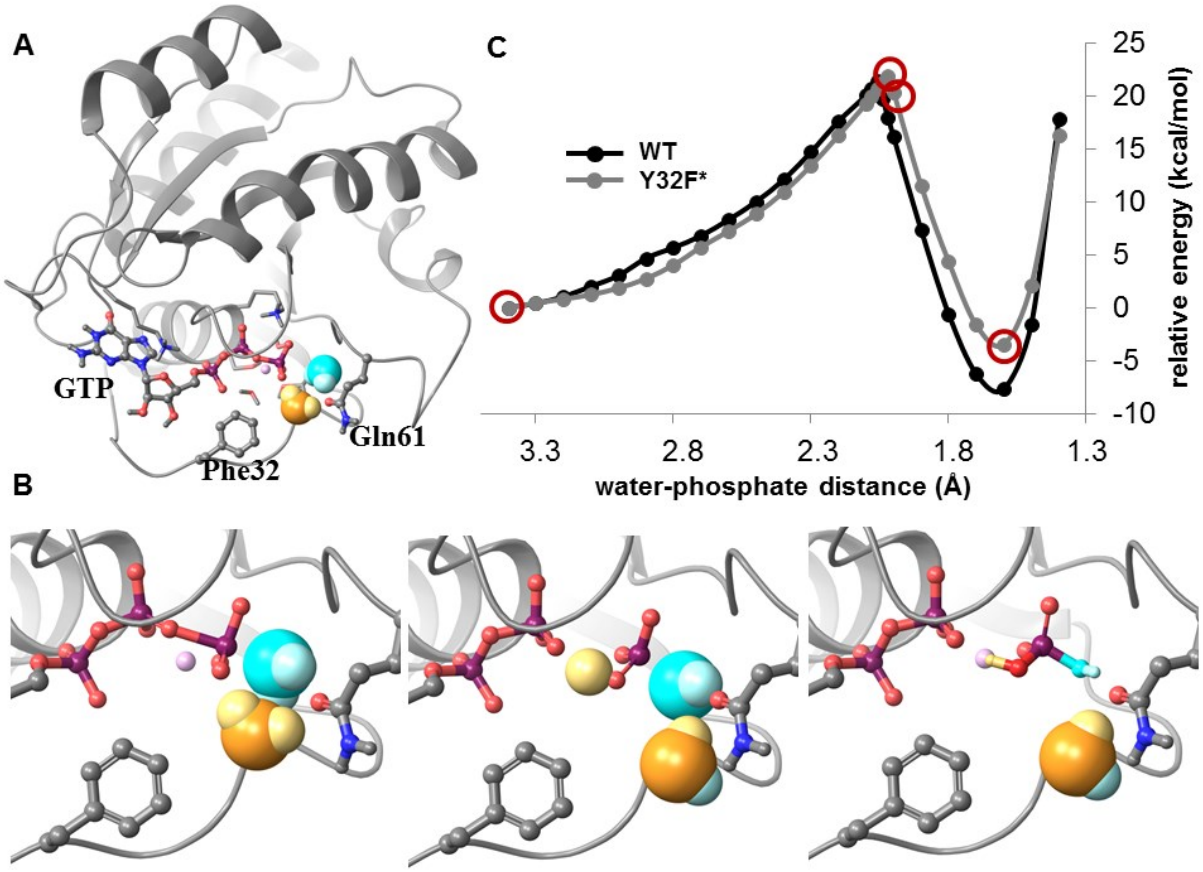

Suppl. Figure 15. Mechanism of the Y32F*-KRAS catalyzed intrinsic GTP-hydrolysis in absence of Tyr32. (**A**) The QM region (Lys16, Ser17, Phe32, Thr35, Gln61, Lys117, Mg^{2+} ion, GTP and 4 water molecules) shown in explicitly – in the reactant state ($r(O_{wat\text{-}catlaytic}\text{-}P_{\gamma\text{-}phosphate}$= 3.4 Å). The catalytic water molecule is shown in cyan, the assisting water in orange. (**B**) Further characteristic points of the scan: r = 2.1 Å (left), r = 2.0 Å (middle) and r = 1.6 Å (right). (**C**) Calculated energies along the profile (points corresponding to stages shown in A. and B are circled in red).

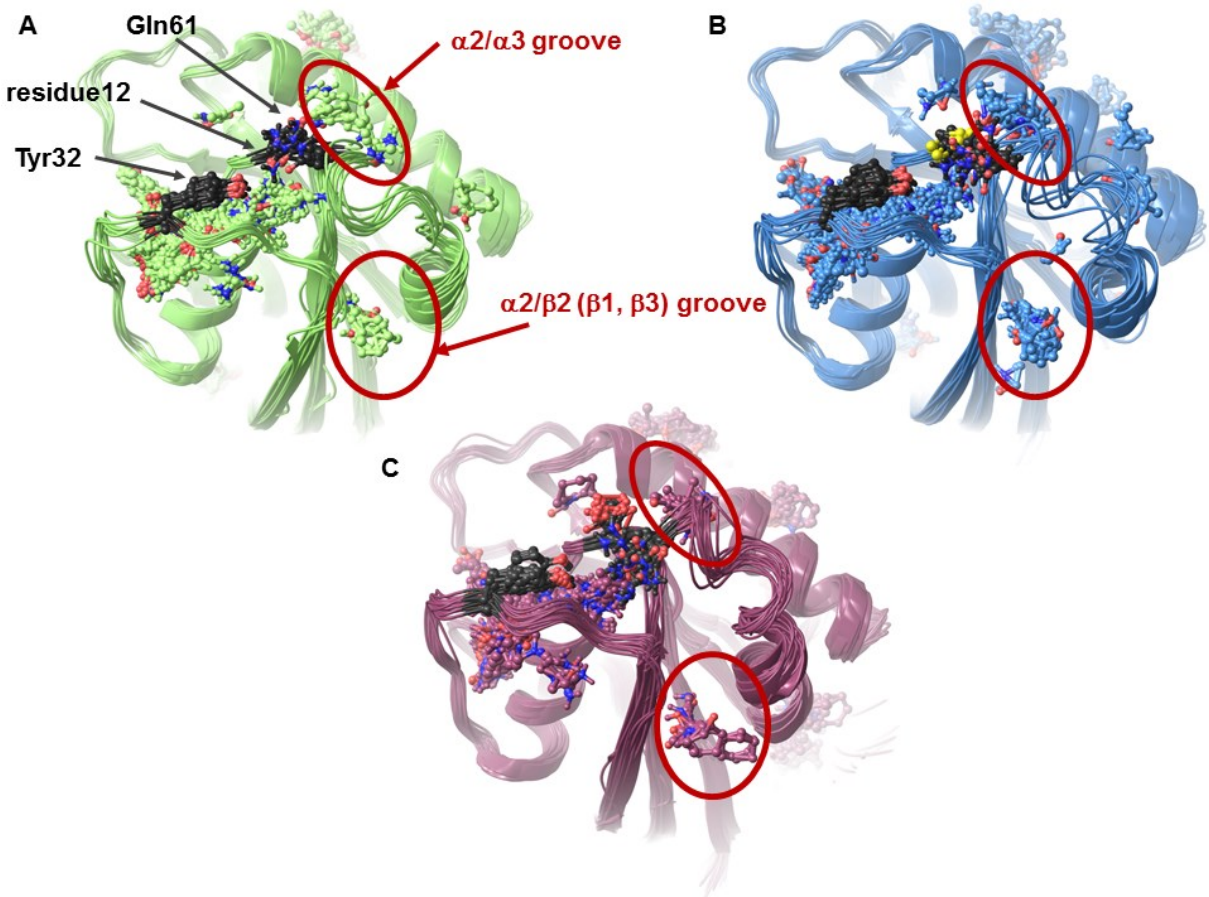

Suppl. Figure 16. Hot spot analysis of the GTP-bound (**A**) WT, (**B**) G12C and (**C**) G12D mutant complexes. FTMAP clusters are shown with the respective probes identified.

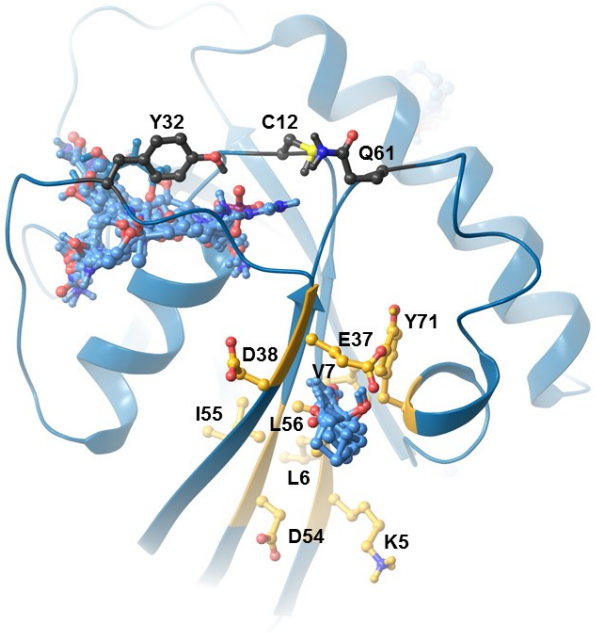

Suppl. Figure 17. Selected structure of the G12C-KRAS-GTP ensemble (see Suppl. Fig. 10B) showing the sidechains identified as the comprising the binding site of a noncovalent allosteric inhibitor discovered recently[1].

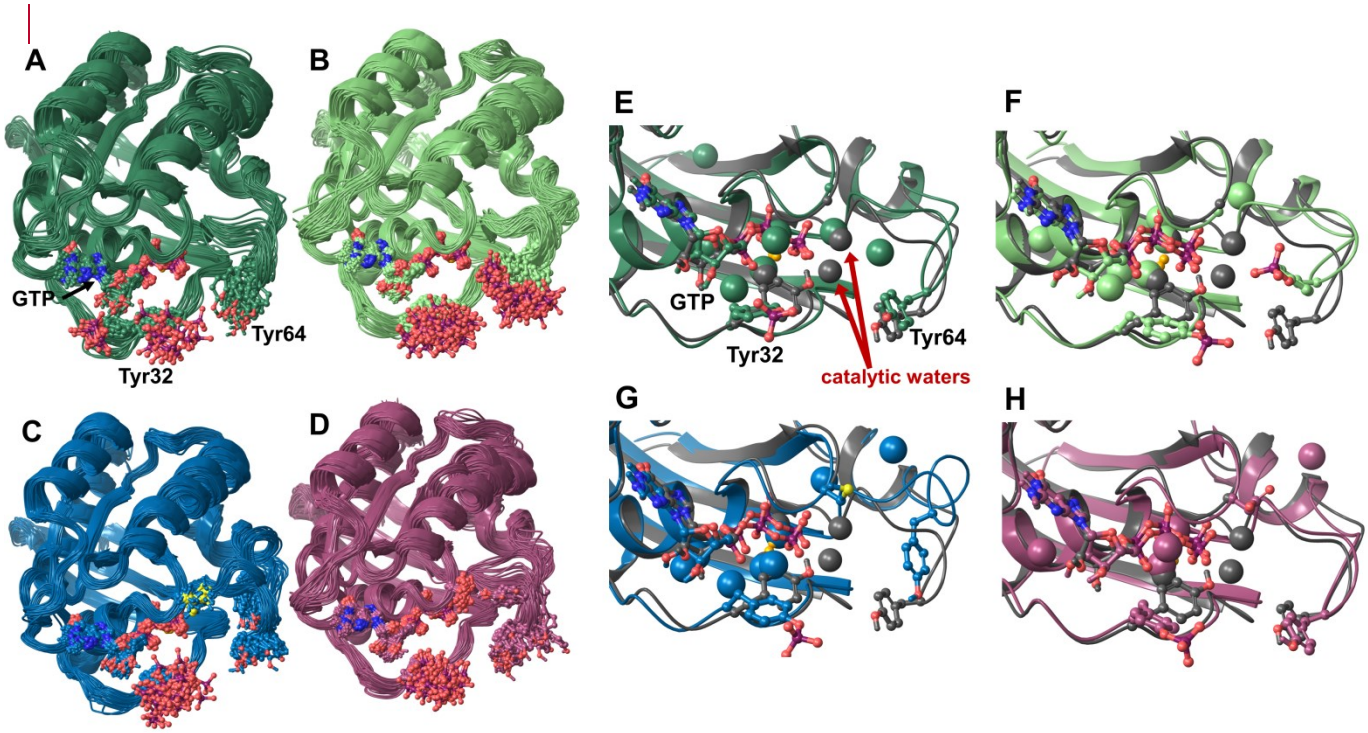

Suppl. Figure 18. The effect of phosphorylation on KRAS-GTP complex structures: results of MD simulations. An overview ((**A**)-(**D**)) showing the mid structures of the most populated clusters (accounting for 90% of all snapshots) of the WT-pY32 (WT at position 12, phosphorylated at Y32; dark green), WT-pY32pY64 (lighter green), G12C-pY32 (blue) and G12D-pY32 (maroon) variants, respectively. ((**E**)-(**H**)): close-up of the nucleotide binding site (average structures of the last 100ns of the equilibrium trajectory, colored as in (A)-(D)) showing low B-fact waters (as spheres of the same color) – overlaid on the WT (un-phosphorylated) structure (shown in gray). Both catalytic waters are only present in the un-phosphorylated structure (gray).

References:

[1] McCarthy, M. J.; Pagba, C. V; Prakash, P.; Naji, A. K.; van der Hoeven, D.; Liang, H.; Gupta, A. K.; Zhou, Y.; Cho, K.-J.; Hancock, J. F.; Gofre, A. A. Discovery of High-Affinity Noncovalent Allosteric KRAS Inhibitors That Disrupt Effector Binding. ACS omega 2019, 4 (2), 2921–2930. https://doi.org/10.1021/acsomega.8b03308

References of the PDB structures shown in the Supporting Information file:

1ctq: Scheidig, A. J.; Burmester, C.; Goody, R. S. The Pre-Hydrolysis State of P21(Ras) in Complex with GTP: New Insights into the Role of Water Molecules in the GTP Hydrolysis Reaction of Ras-like Proteins. Structure 1999, 7 (11), 1311–1324. https://doi.org/10.1016/S0969-2126(00)80021-0.

1qra: Scheidig, A. J.; Burmester, C.; Goody, R. S. The Pre-Hydrolysis State of P21(Ras) in Complex with GTP: New Insights into the Role of Water Molecules in the GTP Hydrolysis Reaction of Ras-like Proteins. Structure 1999, 7 (11), 1311–1324. https://doi.org/10.1016/S0969-2126(00)80021-0.

2rge, 2rgd: Buhrman, G.; Wink, G.; Mattos, C. Transformation Efficiency of RasQ61 Mutants Linked to Structural Features of the Switch Regions in the Presence of Raf. Structure 2007, 15 (12), 1618–1629. https://doi.org/10.1016/j.str.2007.10.011

3gft: to be published

3k8y, 3l8z, 3lbh: Buhrman, G.; Holzapfel, G.; Fetics, S.; Mattos, C. Allosteric Modulation of Ras Positions Q61 for a Direct Role in Catalysis. Proc. Natl. Acad. Sci. U. S. A. 2010, 107 (11), 4931–4936. https://doi.org/10.1073/pnas.0912226107.

3tgp: Accessing protein conformational ensembles using room-temperature X-ray crystallography. Fraser, J.S., van den Bedem, H., Samelson, A.J., Lang, P.T., Holton, J.M., Echols, N., Alber, T. (2011) Proc.Natl.Acad.Sci.USA 108: 16247-16252

4dsn: Maurer, T.; Garrenton, L. S.; Oh, A.; Pitts, K.; Anderson, D. J.; Skelton, N. J.; Fauber, B. P.; Pan, B.; Malek, S.; Stokoe, D.; Ludlam, M. J. C.; Bowman, K. K.; Wu, J.; Giannetti, A. M.; Starovasnik, M. A.; Mellman, I.; Jackson, P. K.; Rudolph, J.; Wang, W.; Fang, G. Small-Molecule Ligands Bind to a Distinct Pocket in Ras and Inhibit SOS-Mediated Nucleotide Exchange Activity. Proc. Natl. Acad. Sci. 2012, 109 (14), 5299–5304. https://doi.org/10.1073/pnas.1116510109.

4efl, 4efm, 4efn: Muraoka, S.; Shima, F.; Araki, M.; Inoue, T.; Yoshimoto, A.; Ijiri, Y.; Seki, N.; Tamura, A.; Kumasaka, T.; Yamamoto, M.; Kataoka, T. Crystal Structures of the State 1 Conformations of the GTP-Bound H-Ras Protein and Its Oncogenic G12V and Q61L Mutants. FEBS Lett. 2012, 586 (12), 1715–1718. https://doi.org/10.1016/j.febslet.2012.04.058.

4lpk, 4l8g: Ostrem, J. M.; Peters, U.; Sos, M. L.; Wells, J. a.; Shokat, K. M. RASG (12C) Inhibitors Allosterically Control GTP Affinity and Effector Interactions Supplementary Information. Nature 2013, 503 (7477), 1–27. https://doi.org/10.1038/nature

4obe, 4ldj: Hunter, J. C.; Gurbani, D.; Ficarro, S. B.; Carrasco, M. A.; Lim, S. M.; Choi, H. G.; Xie, T.; Marto, J. A.; Chen, Z.; Gray, N. S.; Westover, K. D. In Situ Selectivity Profiling and Crystal Structure of SML-8-73-1, an Active Site Inhibitor of Oncogenic K-Ras G12C. Proc. Natl. Acad. Sci. 2014, 111 (24), 8895–8900. https://doi.org/10.1073/pnas.1404639111.

4rsg: Knihtila, R.; Holzapfel, G.; Weiss, K.; Meilleur, F.; Mattos, C. Neutron Crystal Structure of RAS GTPase Puts in Question the Protonation State of the GTP γ-Phosphate. J. Biol. Chem. 2015, 290 (52), 31025–31036. https://doi.org/10.1074/jbc.M115.679860

4ql3, 4tqa, 4tq9, 4wa7: Hunter, J. C.; Manandhar, A.; Carrasco, M. A.; Gurbani, D.; Gondi, S.; Westover, K. D. Biochemical and Structural Analysis of Common Cancer-Associated KRAS Mutations. Mol. Cancer Res. 2015, 13 (9), 1325–1335. https://doi.org/10.1158/1541-7786.MCR-15-0203.

5b2z, 5b30: Matsumoto, S.; Miyano, N.; Baba, S.; Liao, J.; Kawamura, T.; Tsuda, C.; Takeda, A.; Yamamoto, M.; Kumasaka, T.; Kataoka, T.; Shima, F. Molecular Mechanism for Conformational Dynamics of Ras•GTP Elucidated from In-Situ Structural Transition in Crystal. Sci. Rep. 2016, 6. https://doi.org/10.1038/srep25931

5p21: Pai, E. F.; Krengel, U.; Petsko, G. A.; Goody, R. S.; Kabsch, W.; Wittinghofer, A. Refined Crystal Structure of the Triphosphate Conformation of H-Ras P21 at 1.35 A Resolution: Implications for the Mechanism of GTP Hydrolysis. EMBO J. 1990, 9 (8), 2351–2359. https://doi.org/10.1002/j.1460-2075.1990.tb07409.x.

5tb5: Dharmaiah, S.; Bindu, L.; Tran, T. H.; Gillette, W. K.; Frank, P. H.; Ghirlando, R.; Nissley, D. V.; Esposito, D.; McCormick, F.; Stephen, A. G.; Simanshu, D. K. Structural Basis of Recognition of Farnesylated and Methylated KRAS4b by PDEd. Proc. Natl. Acad. Sci. U. S. A. 2016, 113 (44), E6766–E6775. https://doi.org/10.1073/pnas.1615316113

5uk9: Parker, J. A.; Volmar, A. Y.; Pavlopoulos, S.; Mattos, C. K-Ras Populates Conformational States Differently from Its Isoform H-Ras and Oncogenic Mutant K-RasG12D. Structure 2018, 26 (6), 810-820.e4. https://doi.org/10.1016/j.str.2018.03.018.

5us4, 5usj, 5uqw: Welsch, M. E.; Kaplan, A.; Chambers, J. M.; Stokes, M. E.; Bos, P. H.; Zask, A.; Zhang, Y.; Sanchez-Martin, M.; Badgley, M. A.; Huang, C. S.; Tran, T. H., Akkiraju, H., Brown, L. M., Nandakumar, R., Cremers, S., Yang, W. S., Tong, L., Olive, K. P., Ferrando, A., Stockwell, B. R. Multivalent Small-Molecule Pan-RAS Inhibitors. Cell 2017, 168 (5), 878-889.e29. https://doi.org/10.1016/j.cell.2017.02.006.

5vq0, 5vq1, 5vq2, 5vq8, 5vq6, 5vp7, 5vpi, 5vpy, 5pvz, 5w22: Xu, S.; Long, B. N.; Boris, G. H.; Chen, A.; Ni, S.; Kennedy, M. A. Structural Insight into the Rearrangement of the Switch i Region in GTP-Bound G12A K-Ras. Acta Crystallogr. Sect. D Struct. Biol. 2017, 73 (12), 970–984. https://doi.org/10.1107/S2059798317015418.

6asa, 6ase, 6bp1: Lu, J.; Bera, A. K.; Gondi, S.; Westover, K. D. KRAS Switch Mutants D33E and A59G Crystallize in the State 1 Conformation. Biochemistry 2018, 57 (3), 324–333. https://doi.org/10.1021/acs.biochem.7b00974